SI

Supplementary information to:

OPTICAL RESPONSE OF HYPERBOLIC METAMATERIALS WITH ADSORBED NANOPARTICLE ARRAYS

Cristian Zagar[1,2], Ferdinand Krammer[2], John B. Pendry[1], and Alexei A. Kornyshev[2]

[1]Department of Physics, Imperial College London, Blackett Laboratory, South Kensington Campus, SW7 2AZ, London, UK

[2]Department of Chemistry, Imperial College London, Molecular Sciences Research Hub White City Campus, W12 0BZ, UK

5-layer stack model

As presented in this paper HMM are considered to be anisotropic in nature with structure of the HMM being sub wavelength and as such is ignored. The model which is presented here is based of the discrete dipole approximation as presented in refs[1,2,3,4].

The dipole moment of each NP sphere is given by

$$\vec{p} = \hat{a}\left(\vec{E}_0 + \vec{E}_{dip}\right)\#(1)$$

where $\hat{a}$ is the polarizability of the average NP, $\vec{E}_0$ is the external field and $\vec{E}_{dip}$ is the field due to all the oscillating dipoles as $\vec{E}_{dip} = \hat{U}\vec{p}$. As the off-diagonal components of the tensor are 0, and the fields are decoupled the parallel and perpendicular moments can be expressed as

$$p_{\parallel} = \frac{E_{0,\parallel}a_{\parallel}}{1 - \frac{1}{2}a_{\parallel}U_{\parallel}}\#(2)$$

$$p_{\perp} = \frac{E_{0,\perp}a_{\perp}}{1 + a_{\perp}U_{\perp}}\#(3)$$

as it is assumed that the NP layer is an effective anisotropic layer; the parallel and perpendicular components of the permittivity can be calculated using the tangential component of the electric field and the normal component of the displacement. Since $\hat{U}$ has only diagonal elements ($U_{\parallel}$, $U_{\parallel}$ and $U_{\perp}$ in this order), the effective polarizability of the NP layer to be calculated by

$$\beta_{\parallel} = \frac{a_{\parallel}}{1 - \frac{a_{\parallel}}{2}U_{\parallel}}\#(4)$$

SI

$$\beta_{\perp} = \frac{a_{\perp}}{1 + a_{\perp} U_{\perp}} \#(5)$$

so as to calculate the effect of the isotropic material for an anisotropic material above which the NP layer is formed at the height where the point dipole moment is calculated. As the displacement field according to Maxwell's equations is

$$D = \varepsilon_{\perp} E_{\perp} + \varepsilon_{\parallel} E_{\parallel} \#(6)$$

this allows the potential to then be calculated using Poisson's equation

$$\nabla^2 \phi = -\frac{\rho}{\epsilon_0 \epsilon} \#(7)$$

this allows the conditions in each phase to be calculated with the HMM phase needing it to be split in to a parallel and perpendicular component as

$$\frac{\partial^2 \phi_1}{\partial R^2} + \frac{\partial^2 \phi_1}{\partial z^2} = -\frac{\rho}{\epsilon_0 \varepsilon} \#(8)$$

$$\varepsilon_{\parallel} \frac{\partial^2 \phi_2}{\partial R^2} + \varepsilon_{\perp} \frac{\partial^2 \phi_2}{\partial z^2} = 0 \#(9)$$

to this the boundary conditions for a continuous potential across the interface are applied

$$\phi_{1(z=0)} = \phi_{2(z=0)} \#(10)$$

$$\varepsilon \frac{\partial \phi_1}{\partial z}_{(z=0)} = \varepsilon_{\perp} \frac{\partial \phi_2}{\partial z}_{(z=0)} \#(11)$$

using Fourier space the potential in both phases due to a point charge above an anisotropic medium is found to be

$$\phi_1 = \frac{q}{4\pi\epsilon_0 \varepsilon} \left(\frac{\varepsilon - \sqrt{\varepsilon_{\perp} \varepsilon_{\parallel}}}{\varepsilon + \sqrt{\varepsilon_{\perp} \varepsilon_{\parallel}}} \right) \frac{1}{\sqrt{R^2 + (z + z_0)^2}} + \frac{q}{4\pi\epsilon_0 \varepsilon} \frac{1}{\sqrt{R^2 + (z - z_0)^2}} \#(12)$$

$$\phi_2 = \frac{q}{4\pi\epsilon_0 \varepsilon} \left(\frac{2\varepsilon}{\varepsilon + \sqrt{\varepsilon_{\perp} \varepsilon_{\parallel}}} \right) \frac{1}{\sqrt{R^2 + \left(z_0 - z \sqrt{\frac{\varepsilon_{\parallel}}{\varepsilon_{\perp}}} \right)^2}} \#(13)$$

This allows the potential of a point dipole above the anisotropic medium to be calculated as

$$\phi = \frac{qd}{4\pi\varepsilon_0\varepsilon}\left(\frac{\varepsilon - \sqrt{\varepsilon_\perp \varepsilon_\parallel}}{\varepsilon + \sqrt{\varepsilon_\perp \varepsilon_\parallel}}\right)\left(\frac{\cos(\theta)\left((z-z_0)^2+R^2\right)^{\frac{1}{2}} - 2z\cos(\psi)}{\left((z+z_0)^2+R^2\right)^{\frac{3}{2}}}\right) + \frac{qd}{4\pi\varepsilon_0\varepsilon}\left(\frac{\cos(\theta)}{\left((z-z_0)^2+R^2\right)}\right)\#(14)$$

as the only difference here between that of the potential of a point dipole above an isotropic medium and an anisotropic medium is that of the image charge screening factor given by $\frac{\varepsilon - \sqrt{\varepsilon_\perp \varepsilon_\parallel}}{\varepsilon + \sqrt{\varepsilon_\perp \varepsilon_\parallel}}$ in the model presented in refs 2 and 4 and laid out in the main text. Another major change in the model is the split of the wavevector into two components (parallel and perpendicular) inside the HMM. In turn, the parallel and perpendicular dielectric functions of the HMM are modelled using the Maxwell-Garnett approach, as mentioned in the main text.

Comparison of five-layer stack model against results generated by COMSOL Multiphysics

The numerical simulations performed in COMSOL Multiphysics are full wave simulations, where the electromagnetic field is computed inside a cuboid unit cell. The unit cell of a hexagonal NP array contains two NPs. It is the closest idealized version of the real NP arrangement in an adsorbed array where NPs repel each other. The XY cross section of the simulation cell corresponds to the 2d unit cell of a hexagonal lattice, while the Z axis was taken as the direction of light propagation. Therefore, the top and bottom faces were modelled as 'port-boundaries' (in the terminology of COMSOL), while the four surrounding faces were defined as periodic boundaries (Floquet periodicity) in order to replicate the effects of an infinite hexagonal array.

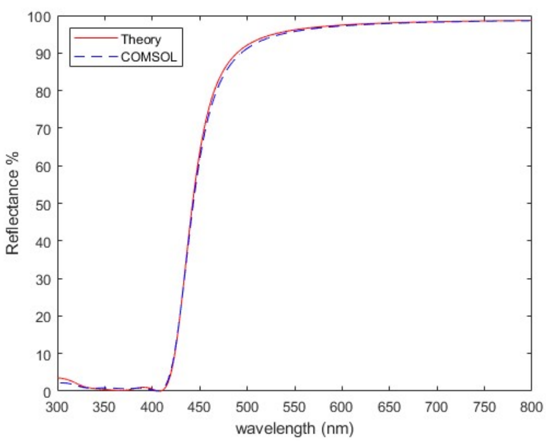

Figure S1: Comparison of 5-Layer stack model results for the reflectivity for HMM (red solid) with COMSOL simulations (blue dash) in the absence of NPs

In the absence of NP above the HMM it is seen that the results formed by the model are in good agreement with those generated form numerical simulations

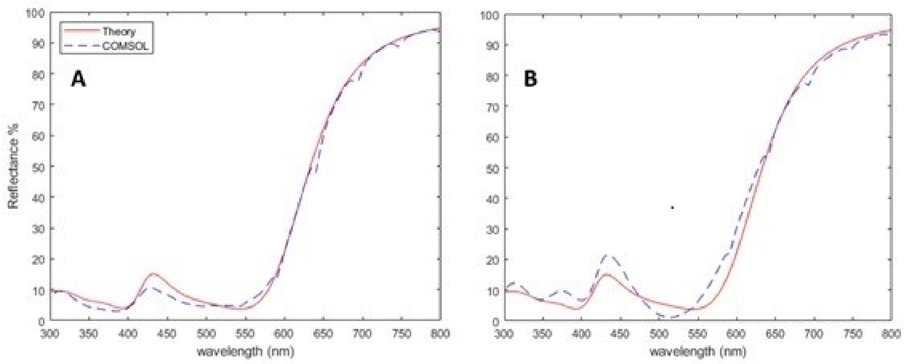

Figure S2: Comparison of 5-layer stack model (red) with differently ordered Ag/TiO_2 HMM in COMSOL simulations (blue dash) with Au NPs present above multilayer Ag/TiO_2 HMM thickness 200 nm. In the COMSOL simulations **(A)** corresponds to the case where Ag is the top sheet of the HMM and **(B)** to the case where the top sheet is TiO_2. Curves plotted for stacked multi-sheet Ag/TiO_2 HMM correspond to a fill-fraction of 50%. Au NP radius R=20 nm, h_s=5 nm a=3R. In COMSOL simulations each sheet has a thickness of 5 nm with a total of 40 sheets.

As a crucial observation, the graphs in fig. S2 show a high absorption broad band (incredibly low reflectance) in the 500-560 nm range. This is fully supported by fig. 5 a) of the main text, where one can see that at this wavelength the electric field practically does not penetrate into the HMM, as light is strongly absorbed exciting the hot spots between NPs and between NPs and the substrate.

It is seen that when the top sheet of the HMM is metallic, the results from the model are in close agreement with those from the numerical COMSOL simulations. However, the results produced when the top sheet is dielectric show some discrepancies, therefore it would be better to use a 6 layer stack model, in which the top sheet of the HMM is treated as a separate layer.

6-layer stack model

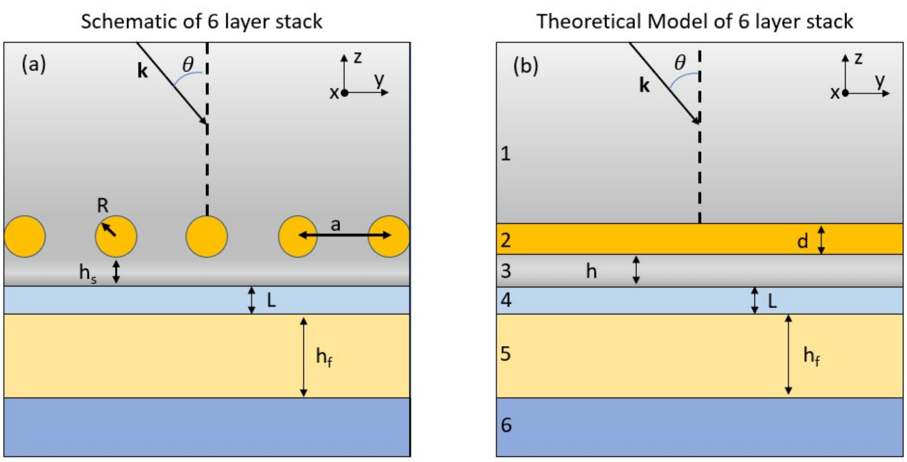

Figure S3: 6-Layer stack model. (a) is the Schematic of the 6-Layer stack model **(b)** the Model used to predict the optical response

SI

Similarly to the 5-layer model, the inclusion of an additional layer –the top sheet of the HMM, will require to recalculate $U_{\perp}$ and $U_{\parallel}$ as we do below. Using Poisson's equations

$$\frac{\partial^2 \phi_1}{\partial R^2} + \frac{\partial^2 \phi_1}{\partial z^2} = -\frac{\rho}{\varepsilon_0 \varepsilon}$$

$$\frac{\partial^2 \phi_2}{\partial R^2} + \frac{\partial^2 \phi_2}{\partial z^2} = 0$$

$$\varepsilon_{\parallel} \frac{\partial^2 \phi_3}{\partial R^2} + \varepsilon_{\perp} \frac{\partial^2 \phi_3}{\partial z^2} = 0$$

and applying the boundary conditions

$$\phi_1(\vec{R}, z = 0) = \phi_2(\vec{R}, z = 0) \#(15)$$

$$\phi_2(\vec{R}, z = -h) = \phi_3(\vec{R}, z = -h) \#(16)$$

$$\varepsilon \frac{\partial \phi_1}{\partial z}\Big|_{z=0} = \varepsilon_2 \frac{\partial \phi_2}{\partial z}\Big|_{z=0} \#(17)$$

$$\varepsilon_2 \frac{\partial \phi_2}{\partial z}\Big|_{z=-h} = \varepsilon_{\perp} \frac{\partial \phi_3}{\partial z}\Big|_{z=-h} \#(18)$$

for the Fourier-Bessel transform of the potential of a point charge above this anisotropic medium we get:

$$\hat{\phi}_1 = \frac{\left(\frac{\varepsilon_2 - \sqrt{\varepsilon_{\perp}\varepsilon_{\parallel}}}{\varepsilon_2 + \sqrt{\varepsilon_{\perp}\varepsilon_{\parallel}}}\right)}{1 - \left(\frac{\varepsilon_2 - \sqrt{\varepsilon_{\perp}\varepsilon_{\parallel}}}{\varepsilon_2 + \sqrt{\varepsilon_{\perp}\varepsilon_{\parallel}}}\right)\left(\frac{\varepsilon_2 - \varepsilon}{\varepsilon_2 + \varepsilon}\right) e^{-2Kh}} k_0 \frac{e^{-K(z_0 + z + 2h)}}{K} - k_0 \frac{e^{-K(z + z_0)}}{K} \frac{\ldots}{1 - \left(\frac{\varepsilon_2 - \sqrt{\ldots}}{\varepsilon_2 + \sqrt{\ldots}}\right) \ldots}$$

When transforming back to real space we encounter 3 integrals, all of the following type

$$\int_0^{\infty} \frac{e^{-qx}}{1 - a e^{-px}} dx.$$

Contour integration gives an identity:

SI

$$\int_0^\infty \frac{e^{-qx}}{1-ae^{-px}}dx = \Sigma_{k=0}^{\infty}\frac{a^k}{q+kp}, \qquad [|a|<1]$$

Thus, the potential of the point charge above the HMM with a thin layer above is

$$\phi_1 = k_0\left(\frac{\varepsilon_2 - \sqrt{\varepsilon_\parallel \varepsilon_\perp}}{\varepsilon_2 + \sqrt{\varepsilon_\parallel \varepsilon_\perp}}\right)\Sigma_{k=0}^{\infty}\frac{\left(\left(\frac{\varepsilon_2 - \sqrt{\varepsilon_\parallel \varepsilon_\perp}}{\varepsilon_2 + \sqrt{\varepsilon_\parallel \varepsilon_\perp}}\right)\left(\frac{\varepsilon_2 - \varepsilon_1}{\varepsilon_2 + \varepsilon_1}\right)\right)^k}{\sqrt{(z_0 + z + 2h(1+k))^2 + R^2}} + k_0\left(\frac{\varepsilon_2 - \varepsilon_1}{\varepsilon_2 + \varepsilon_1}\right)\Sigma_{k=0}^{\infty}\frac{\left(\left(\frac{\varepsilon_2 -}{\varepsilon_2 +}\right.\right.}{\sqrt{(z}} \; k_0\frac{1}{\sqrt{R^2 + (z - z_0)^2}} \qquad (20)$$

This holds as long as the condition $\left|\left(\frac{\varepsilon_L - \sqrt{\varepsilon_\perp \varepsilon_\parallel}}{\varepsilon_L + \sqrt{\varepsilon_\perp \varepsilon_\parallel}}\right)\left(\frac{\varepsilon_L - \varepsilon}{\varepsilon + \varepsilon_L}\right)\right| < 1$ is satisfied. This only holds true if the top sheet is a dielectric. The potential created by a point dipole sitting at a height z_0 above the interface, oriented at an angle ψ with respect to the normal to the interfacial plane, i.e. z-axis, and an angle θ from the vector between the dipole and the point at which the potential is calculated; R and z are the cylindrical coordinates of the said point.

$$\phi_{tot} = pk_0\frac{\left(\varepsilon_L - \sqrt{\varepsilon_\parallel \varepsilon_\perp}\right)}{\left(\varepsilon_L + \sqrt{\varepsilon_\parallel \varepsilon_\perp}\right)}\Sigma_{n=0}^{\infty}\left(\frac{\left(\varepsilon_L - \sqrt{\varepsilon_\parallel \varepsilon_\perp}\right)(\varepsilon_L - \varepsilon)}{\left(\varepsilon_L + \sqrt{\varepsilon_\parallel \varepsilon_\perp}\right)(\varepsilon_L + \varepsilon)}\right)^n\left(\frac{-\cos(\psi)(2z + 2h(1+n)) +}{\left((z_0 + z + 2h(1+\right.}\right.$$

$$+ pk_0\frac{(\varepsilon - \varepsilon_L)}{(\varepsilon + \varepsilon_L)}\Sigma_{n=0}^{\infty}\left(\frac{\left(\varepsilon_L - \sqrt{\varepsilon_\parallel \varepsilon_\perp}\right)(\varepsilon_L - \varepsilon)}{\left(\varepsilon_L + \sqrt{\varepsilon_\parallel \varepsilon_\perp}\right)(\varepsilon_L + \varepsilon)}\right)^n \left(\frac{-\cos(\psi)(2z + 2hn) + \left(R^2 + (z_0 - z)^2\right)^{\frac{1}{2}}\cos\theta}{\left((z_0 + z + 2hn)^2 + R^2\right)^{\frac{3}{2}}}\right) + pk_0\left(\frac{\cos\theta}{\left(R^2 + (z - z_0)^2\right)}\right) \qquad (21$$

For $U_\parallel$ and $U_\perp$ we get

$$U_{\perp} = \Sigma_j \left[k_0 \frac{\left(\varepsilon_L - \sqrt{\varepsilon_{\parallel}\varepsilon_{\perp}}\right)}{\left(\varepsilon_L + \sqrt{\varepsilon_{\parallel}\varepsilon_{\perp}}\right)} \Sigma_{n=0}^{\infty} \left(\frac{\left(\varepsilon_L - \sqrt{\varepsilon_{\parallel}\varepsilon_{\perp}}\right)(\varepsilon_L - \varepsilon)}{\left(\varepsilon_L + \sqrt{\varepsilon_{\parallel}\varepsilon_{\perp}}\right)(\varepsilon_L + \varepsilon)} \right)^n \left(\frac{1}{a^3\left(\frac{4(z+h(1+n))^2}{a^2} + |r_j|^2\right)^{\frac{3}{2}}} - \frac{}{a^5\left(\right.} \right. \right. \tag{22}$$

$$U_{\parallel} = \Sigma_{ij} \left[k_0 \frac{\left(\varepsilon_L - \sqrt{\varepsilon_{\parallel}\varepsilon_{\perp}}\right)}{\left(\varepsilon_L + \sqrt{\varepsilon_{\parallel}\varepsilon_{\perp}}\right)} \Sigma_{n=0}^{\infty} \left(\frac{\left(\varepsilon_L - \sqrt{\varepsilon_{\parallel}\varepsilon_{\perp}}\right)(\varepsilon_L - \varepsilon)}{\left(\varepsilon_L + \sqrt{\varepsilon_{\parallel}\varepsilon_{\perp}}\right)(\varepsilon_L + \varepsilon)} \right)^n \left(\frac{1}{a^3\left(\frac{4(z+h(1+n))^2}{a^2} + |r_{ij}|^2\right)^{\frac{3}{2}}} - \frac{}{2a^3} \right. \right. \tag{23}$$

These can then be substituted into the expression for the effective polarizability of the NP layer as presented in equations (4) and (5), giving us—

$$\beta_{\parallel} = \frac{\chi(\omega)}{1 - \chi(\omega)\frac{1}{2\varepsilon_1}\left\{ \begin{aligned} &\frac{U_A}{a^3} + \xi_2(\omega)\sum_{n=0}^{\infty}\left[(\xi_1(\omega)\xi_2(\omega))^n\left(\frac{f(h_2,a)}{a^3} - \frac{3}{2}\frac{g_1(h_2,a)}{a^3} + \frac{1}{8h_2^3}\right)\right] \\ &-\xi_1(\omega)\sum_{n=0}^{\infty}\left[(\xi_1(\omega)\xi_2(\omega))^n\left(\frac{f(h_1,a)}{a^3} - \frac{3}{2}\frac{g_1(h_1,a)}{a^3} + \frac{1}{8h_1^3}\right)\right] \end{aligned} \right\}} \#(25)$$

$$\beta_{\perp}(\omega) = \frac{\chi(\omega)}{1 + \chi(\omega)\frac{1}{\varepsilon_1}\left[\begin{aligned} &\frac{U_A}{a^3} + \xi_2(\omega)\sum_{n=0}^{\infty}\left[(\xi_1(\omega)\xi_2(\omega))^n\left(\frac{f(h_2,a)}{a^3} - 12\frac{h^2 g_2(h_2,a)}{a^5} - \frac{1}{4h_2^3}\right)\right] \\ &-\xi_1(\omega)\sum_{n=0}^{\infty}\left[(\xi_1(\omega)\xi_2(\omega))^n\left(\frac{f(h_1,a)}{a^3} - 12\frac{h^2 g_2(h_1,a)}{a^5} - \frac{1}{4h_1^3}\right)\right] \end{aligned} \right]} \#(26)$$

where $\chi(\omega)$ is the polarizability of each NP as given in the main text,

$$\xi_1(\omega) = \frac{\varepsilon_4 - \varepsilon_3}{\varepsilon_4 + \varepsilon_3}, \qquad \xi_2(\omega) = \frac{\varepsilon_4 - \sqrt{\varepsilon_5^{\parallel}(\omega)\varepsilon_5^{\perp}(\omega)}}{\varepsilon_4 + \sqrt{\varepsilon_5^{\parallel}(\omega)\varepsilon_5^{\perp}(\omega)}}, \qquad h_1 = h + Ln, h_2 = h + L(n+1)$$

this allows the 6-layer model to be described by figure S3, where layer 1 is bulk dielectric with a permittivity of ε_1, layer 2 is made of an array of NPs with a thickness of d as given by equation 38, layer 3 is a spacer layer of thickness h_s with a permittivity $\varepsilon_3 = \varepsilon_1$. Layer 4, which is the layer above the HMM, has a permittivity of ε_4 with a thickness of L, layer 5 is the HMM with a thickness of h_f and a parallel (perpendicular) permittivity of $\varepsilon^{\parallel}_{4}(\omega)$ $\left(\varepsilon^{\perp}_{4}(\omega)\right)$ which is given by equation 1(2) of the main text. Layer 6 is the material which the HMM is mounted on (normally glass) with a permittivity of ε_6.

The total transfer matrix is calculated by $\tilde{M} = \tilde{M}_1 \cdot \tilde{M}_2 \cdot \tilde{M}_3 \cdot \tilde{M}_4 \cdot \tilde{M}_5$

$$\tilde{M} = \frac{1}{t_{1,2}t_{2,3}t_{2,3}t_{4,5}t_{5,6}}\begin{pmatrix} e^{-i\delta_2} & r_{1,2}e^{i\delta_2} \\ r_{1,2}e^{-i\delta_2} & e^{i\delta_2} \end{pmatrix}\begin{pmatrix} e^{-i\delta_3} & r_{2,3}e^{i\delta_3} \\ r_{2,3}e^{-i\delta_3} & e^{i\delta_3} \end{pmatrix}\begin{pmatrix} e^{-i\delta_4} & r_{3,4}e^{i\delta_4} \\ r_{3,4}e^{-i\delta_4} & e^{i\delta_4} \end{pmatrix}\Bigg(\quad (27)$$

where the phase shifts are given by $\delta^{\parallel,\perp}_{2} = k^{\parallel,\perp}_{2} d, \delta_3 = k_3 h_s, \ \delta_4 = k_4 L$ and $\delta^{\parallel,\perp}_{5} = k^{\parallel,\perp}_{5} h_f$, with the reflection and transmittance coefficients presented in the main text. The wave vector components are given by

$$k_1(\omega) = \frac{\omega}{c}\sqrt{\varepsilon_1} cos\theta \qquad \#(28)$$

$$k^{\parallel}_{2}(\omega) = \frac{\omega}{c}\sqrt{\varepsilon^{\parallel}_{2}(\omega) - \varepsilon_1 \sin^2\theta} \ \#(29)$$

$$k^{\perp}_{2}(\omega) = \frac{\omega}{c}\left(\frac{\varepsilon^{\parallel}_{2}(\omega)}{\varepsilon^{\perp}_{2}(\omega)}\right)^{\frac{1}{2}}\sqrt{\varepsilon^{\perp}_{2}(\omega) - \varepsilon_1 \sin^2\theta}\#(30)$$

$$k_3(\omega) = \frac{\omega}{c}\sqrt{\varepsilon_3(\omega) - \varepsilon_1 \sin^2\theta} \qquad \#(31)$$

$$k_4(\omega) = \frac{\omega}{c}\sqrt{\varepsilon_4(\omega) - \varepsilon_1 \sin^2\theta} \qquad \#(32)$$

$$k^{\parallel}_{5}(\omega) = \frac{\omega}{c}\sqrt{\varepsilon^{\parallel}_{5}(\omega) - \varepsilon_1 \sin^2\theta} \qquad \#(33)$$

$$k^{\perp}_{5}(\omega) = \frac{\omega}{c}\left(\frac{\varepsilon^{\parallel}_{5}(\omega)}{\varepsilon^{\perp}_{5}(\omega)}\right)^{\frac{1}{2}}\sqrt{\varepsilon^{\perp}_{5}(\omega) - \varepsilon_1 \sin^2\theta} \qquad \#(34)$$

$$k_6(\omega) = \frac{\omega}{c}\sqrt{\varepsilon_6(\omega) - \varepsilon_1 \sin^2\theta} \qquad \#(35)$$

Equations (17), (18) and (19) form the main text can be used to determine the reflectance, transmittance and absorption.

Comparison of 6 layer stack model against results generated by COMSOL Multiphysics

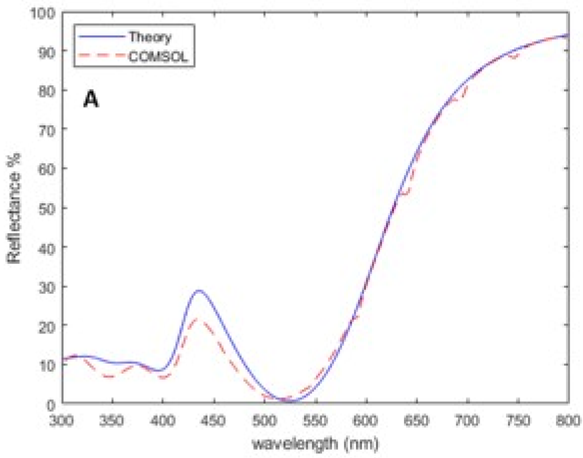

Figure S4: Comparison of the reflectance at normal incidence calculated within the 6-layer stack model (red), with COMSOL simulations (blue dash). Moving to the 6-layer model introduces an additional dielectric layer above the anisotropic material. This layer represents the top sheet of HMM, the rest of it modelled by the Maxwell-Garnett model as a homogenous anisotropic material. We consider Ag/TiO_2 HMM with a fill fraction of 50%, h_f=200 nm. Other parameters: Au NP $R = 20\ nm\ a = 3R\quad hs = 1\ nm$, $\varepsilon_1 = \varepsilon_3 = 1.78$, $\varepsilon_5 = 2.25$. HMM treated in COMSOL as 40 layers each 5nm thick.

NP-array-modified Fabry-Perot interferometer: the model and basic equations

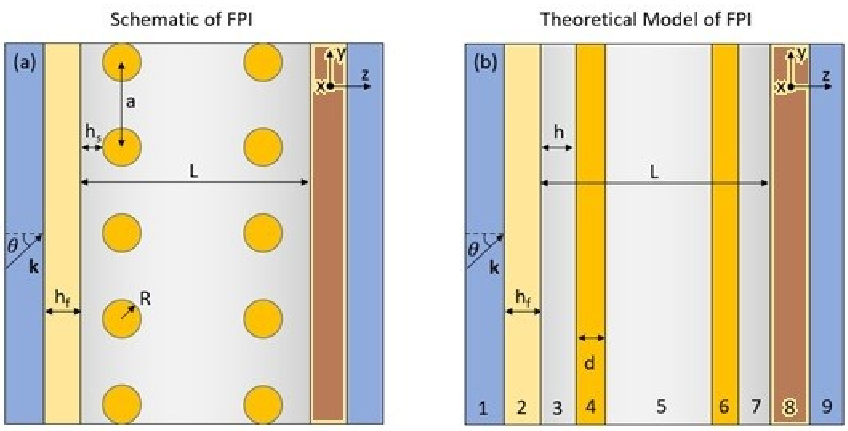

Figure S5: Nine-Layer stack model representing a Fabry-Perot cell. (a) is the schematic of the cell and **(b)** the model used to predict the optical response.

This model is an extension of that presented in Refs 5 and 6 with the right “mirror” being anisotropic in nature and the left “mirror” being isotropic in nature

$$\tilde{M} = \frac{1}{t_{1,2}}\begin{pmatrix} e^{-i\delta_2} & r_{1,2}e^{i\delta_2} \\ r_{1,2}e^{-i\delta_2} & e^{i\delta_2} \end{pmatrix}\cdot\frac{1}{t_{2,3}}\begin{pmatrix} e^{-i\delta_3} & r_{2,3}e^{i\delta_3} \\ r_{2,3}e^{-i\delta_3} & e^{i\delta_3} \end{pmatrix}\cdot\frac{1}{t_{3,4}}\begin{pmatrix} e^{-i\delta_4} & r_{3,4}e^{i\delta_4} \\ r_{3,4}e^{-i\delta_4} & e^{i\delta_4} \end{pmatrix}\cdot\frac{1}{t_{4,5}} \begin{pmatrix} e^{-i\delta_6} & r_{5,6}e^{i\delta_6} \\ r_{5,6}e^{-i\delta_6} & e^{i\delta_6} \end{pmatrix}\cdot\frac{1}{t_{6,7}}\begin{pmatrix} e^{-i\delta_7} & r_{6,7}e^{i\delta_7} \\ r_{6,7}e^{-i\delta_7} & e^{i\delta_7} \end{pmatrix}\cdot\frac{1}{t_{7,8}}\begin{pmatrix} e^{-i\delta_8} & r_{7,8}e^{i\delta_8} \\ r_{7,8}e^{-i\delta_8} & e^{i\delta_8} \end{pmatrix}\cdot\frac{1}{t_{8,9}}\begin{pmatrix} 1 \\ r_{8,9} \end{pmatrix} \quad (36)$$

Where the phase shifts are $\delta_2 = k_2 h_{f1}$, $\delta_3 = k_3 h_s$, $\delta^{\parallel,\perp}_4 = k^{\parallel,\perp}_4 d$, $\delta_5 = k_5(L - 2h_s - 2d)$, $\delta^{\parallel,\perp}_6 = k^{\parallel,\perp}_6 d$, $\delta_7 = k_7 h_s$ and $\delta^{\parallel,\perp}_8 = k^{\parallel,\perp}_8 h_{f2}$. With the wave vectors of the individual layers as:

$$k_1(\omega) = \frac{\omega}{c}\sqrt{\varepsilon_1} cos\theta \quad (37)$$

$$k_2(\omega) = \frac{\omega}{c}\sqrt{\varepsilon_2(\omega) - \varepsilon_1 \sin^2\theta} \quad (38)$$

$$k_3(\omega) = \frac{\omega}{c}\sqrt{\varepsilon_3(\omega) - \varepsilon_1 \sin^2\theta} \quad (39)$$

$$k^{\parallel}_4(\omega) = \frac{\omega}{c}\sqrt{\varepsilon^{\parallel}_4(\omega) - \varepsilon_1 \sin^2\theta} \quad (40)$$

$$k^{\perp}_4(\omega) = \frac{\omega}{c}\left(\frac{\varepsilon^{\parallel}_4(\omega)}{\varepsilon^{\perp}_4(\omega)}\right)^{\frac{1}{2}}\sqrt{\varepsilon^{\perp}_4(\omega) - \varepsilon_1 \sin^2\theta} \quad (41)$$

$$k_5(\omega) = \frac{\omega}{c}\sqrt{\varepsilon_5(\omega) - \varepsilon_1 \sin^2\theta} \quad (42)$$

$$k^{\parallel}_6(\omega) = \frac{\omega}{c}\sqrt{\varepsilon^{\parallel}_6(\omega) - \varepsilon_1 \sin^2\theta} \quad (43)$$

$$k^{\perp}_6(\omega) = \frac{\omega}{c}\left(\frac{\varepsilon^{\parallel}_6(\omega)}{\varepsilon^{\perp}_6(\omega)}\right)^{\frac{1}{2}}\sqrt{\varepsilon^{\perp}_6(\omega) - \varepsilon_1 \sin^2\theta} \quad (44)$$

$$k_7(\omega) = \frac{\omega}{c}\sqrt{\varepsilon_7(\omega) - \varepsilon_1 \sin^2\theta} \quad (45)$$

$$k^{\parallel}_8(\omega) = \frac{\omega}{c}\sqrt{\varepsilon^{\parallel}_8(\omega) - \varepsilon_1 \sin^2\theta} \quad (46)$$

$$k^{\perp}_8(\omega) = \frac{\omega}{c}\left(\frac{\varepsilon^{\parallel}_8(\omega)}{\varepsilon^{\perp}_8(\omega)}\right)^{\frac{1}{2}}\sqrt{\varepsilon^{\perp}_8(\omega) - \varepsilon_1 \sin^2\theta} \quad (47)$$

$$k_9(\omega) = \frac{\omega}{c}\sqrt{\varepsilon_9(\omega) - \varepsilon_1 \sin^2\theta} \quad (48)$$

Equations (17), (18) and (19) form the main text can be used to determine the reflectance, transmittance and absorption. The complete results can be observed below.

References

1. Flatte, M. E., Kornyshev, A. A. & Urbakh, M. Electrovariable Nanoplasmonics and Self-Assembling Smart Mirrors. *J. Phys. Chem.* **C 114**, 1735–1747 (2010).
2. D. Sikdar, S. B. Hasan, M. Urbakh, J. B. Edel and A. A. Kornyshev, *Physical Chemistry Chemical Physics*, 2016, **18**, 20486–20498.
3. Persson, B, N, J. & Liebsch, A. Optical properties of two-dimensional systems of randomly distributed particles. *Phys. Rev.* **B 28**, 4247–4254 (1983)
4. Paget, J. et al. Optical Properties of Ordered Self-Assembled Nanoparticle Arrays at Interfaces. *J. Phys. Chem.* **C 118**, 23264–23273 (2014).
5. Weir, H., Edel, J. B., Kornyshev, A. A. & Sikdar, D. Towards Electrotuneable Nanoplasmonic Fabry – Perot Interferometer. *Sci. Rep.* **8**, # 565 (2018).
6. Sikdar, D. & Kornyshev, A. A. An electro-tunable Fabry – Perot interferometer based on dual mirror-on-mirror nanoplasmonic metamaterials. *Nanophotonics* **8**, 2279–2290 (2019).